DESY 06-041
MPP-2006-57
hep-ph/0606073
June 2006

ISSN 0418-9833

arXiv:hep-ph/0606073v2 17 Oct 2007

Single top production at HERA in the Standard Model and its minimal supersymmetric extension

W. Hollik[a], A. Hüttmann[b]*, B.A. Kniehl[b]

[a] Max-Planck-Institut für Physik (Werner-Heisenberg-Institut),
Föhringer Ring 6, 80805 Munich, Germany

[b] II. Institut für Theoretische Physik, Universität Hamburg,
Luruper Chaussee 149, 22761 Hamburg, Germany

Reveived 7 June 2006

Abstract

The H1 Collaboration at the DESY electron-proton collider HERA has observed, in photoproduction and neutral-current deep-inelastic scattering, an unexpected excess of events with isolated leptons and missing transverse momentum, especially at large values of hadronic transverse momentum—a signature typical for single top-quark production. This observation is being substantiated in the HERA II run. Motivated by this, we evaluate the cross section of single top-quark photo- and electroproduction both in the standard model and its minimal supersymmetric extension, considering both minimal and non-minimal flavour-violation scenarios in the latter case.

PACS numbers: 12.60.Jv, 13.60.Hb, 13.85.Ni, 14.65.Ha

---

*Present address: Deutsches Elektronen-Synchrotron (DESY), Notkestr. 85, 22607 Hamburg, Germany.

1 Introduction

Searches for single top-quark production via the neutral current (NC),

$$e^{\pm}p \to e^{\pm}t + X, \tag{1}$$

have been performed by the H1 Collaboration [1] and the ZEUS Collaboration [2] at the DESY electron-proton collider HERA. The H1 Collaboration found several events, leading to a cross section of $\sigma = 0.29^{+0.15}_{-0.14}$ pb. Alternatively, assuming that the observed events are due to a statistical fluctuation, upper limits of 0.55 pb on σ and of 0.27 on the anomalous $tu\gamma$ coupling $\kappa_{tu\gamma}$ were established at the 95% confidence level (CL). On the other hand, the ZEUS Collaboration found no evidence for top-quark production and was able to place upper bounds of 0.225 pb on σ and of 0.174 on $\kappa_{tu\gamma}$ at 95% CL.

Single top-quark production via the charged current (CC) is possible at the tree level, but its cross section is less than 1 fb [3]. Furthermore, such events can be separated experimentally due to the absence of a scattered electron or positron in the final state.

In this work, we calculate the cross section of process (1) in the standard model (SM) and its minimal supersymmetric (SUSY) extension (MSSM), considering both scenarios with minimal flavour violation (MFV) and non-minimal flavour violation (NMFV). The bulk of the cross section is due to photoproduction and electromagnetic deep-inelastic scattering (DIS), while the contribution due to the exchange of a virtual Z boson is greatly suppressed by its mass. Since photonic interactions cannot change flavour and the top quark does not appear as a parton in the proton, we are dealing here with a loop-induced process. In the SM and the MFV MSSM, its cross section is further suppressed by the smallness of the contributing elements of the Cabibbo-Kobayashi-Maskawa (CKM) matrix. In more general MSSM scenarios, misalignment between the quark and squark sectors can appear, and the CKM matrix is no longer the only source of flavour violation. Thus, the flavour-changing (FC) couplings are not Cabibbo suppressed, and sizeable contributions to FC NC processes can occur. On the other hand, there are strong experimental bounds on squark mixing involving the first generation, coming from data on K^0–$\overline{K}^0$ and D^0–$\overline{D}^0$ mixing [4]. If the squark mixing involving the first generation is neglected completely, there are no new vertices for incoming up-quarks compared to the MFV MSSM. Thus, every new contribution in this scenario is suppressed by the parton distribution function (PDF) of the charm quark in the proton. Because the SM cross section for NC single top-quark production is highly suppressed, every detected event is an indication of physics beyond the SM.

This paper is organised as follows. In Section 2, we describe the analytical calculation of the SM cross section. In Section 3, we outline the theoretical framework of FC interactions in the MSSM. The numerical analysis is presented in Section 4. Our conclusions are summarised in Section 5.

2 SM cross section

In this section, the analytical calculation of the SM cross section is described. As indicated in Fig. 1, we denote the four-momenta of the incoming proton, parton (up or charm quark), and electron by P, p, and k, respectively, and those of the outgoing top quark and electron by p' and k', respectively. As for the centre-of-mass (CM) energy and the top-quark mass, we have $S = (P+k)^2$ and $m_t^2 = (p')^2$. We neglect the masses of the proton, the incoming quarks, and the electron, so that $P^2 = p^2 = k^2 = k'^2 = 0$. The four-momentum of the exchanged photon is given by $q = k - k'$, and, as usual, we introduce the virtuality variable $Q^2 = -q^2 > 0$. The variable $y = (q \cdot P)/(k \cdot P)$ measures the relative electron energy loss in the proton rest frame.

2.1 Electroproduction

Single top-quark production in NC DIS occurs via the partonic subprocess

$$e^\pm q \to e^\pm t, \tag{2}$$

where $q = u, c$. The Feynman diagrams contributing in the SM to process (2) with $q = u$ are depicted in Fig. 2. The ones for $q = c$ are similar. The amplitude of this processes was also calculated in Ref. [5]. There appears at least one off-diagonal element of the CKM matrix in each term. If the contributions of the inner-quark flavours to a single Feynman diagram are added up and their masses are neglected, the amplitude of this Feynman diagram vanishes due to the unitarity of the CKM matrix. Thus, we cannot neglect the inner-quark masses here. Although our choice $m_c = 0 < m_d$ appears unphysical at first sight, it is inconsequential in practice. In fact, we verified that the use of a realistic value of m_c affects our numerical results only insignificantly. A detailed proof of hard-scattering factorisation with the inclusion of heavy-quark masses may be found in Ref. [6].

Our calculation proceeds along the lines of Ref. [7]. The differential cross section of process (2) reads

$$\left(\frac{d\sigma}{dQ^2 dy}\right)_{\text{part}} = \frac{1}{16\pi\xi S}\overline{|\mathcal{M}|^2}\,\delta\left(\xi y S - Q^2 - m_t^2\right), \tag{3}$$

where ξ, defined as $p = \xi P$, is the fraction of the proton momentum passed on to the incoming quark and $\overline{|\mathcal{M}|^2}$ is the squared amplitude averaged (summed) over the spin and colour degrees of freedom of the initial-state (final-state) particles. The kinematically allowed ranges of Q^2 and y are

$$\begin{aligned} Q^2_{\text{cut}} < Q^2 < y_{\max} S - m_t^2, \\ \frac{Q^2 + m_t^2}{S} < y < y_{\max}, \end{aligned} \tag{4}$$

where Q^2_{cut} defines the demarcation between photoproduction and electroproduction and $y_{\max}$ is an experimental acceptance cut. In Ref. [1], values for Q^2_{cut} and $y_{\max}$ are not specified. In our numerical analysis, we employ the typical values $Q^2_{\text{cut}} = 4$ GeV^2 and $y_{\max} = 0.95$. Our numerical results are insensitive to the precise choice of $y_{\max}$ as long it is close to unity. On the other hand, the dependence on Q^2_{cut} approximately cancels out in the combination of photoproduction and electroproduction, as we explicitly verify.

In the parton model of QCD, the hadronic cross section of process (1) is obtained by convoluting the partonic cross section of process (2) with the appropriate PDF $F_q(\xi, \mu_F)$, where μ_F is the factorisation scale, and summing over $q = u, c$, as

$$\left(\frac{d\sigma}{dQ^2 dy}\right)_{\text{hadr}} = \sum_{q=u,c}\int_0^1 d\xi\, F_q(\xi, \mu_F)\left(\frac{d\sigma}{dQ^2 dy}\right)_{\text{part}}. \tag{5}$$

There are two candidate mass scales for μ_F, namely $\sqrt{Q^2}$ and m_t, and the optimal choice is likely to lie somewhere in between, at $\mu_F = \left(\sqrt{Q^2} + m_t\right)/2$ say. At any rate, we have $\mu_F \gg m_c$, so that charm is an active quark flavour in the initial state, contributing at full strength via its PDF.

The expression for $\overline{|\mathcal{M}|^2}$ of process (2) may be decomposed into a hadronic tensor $H^{\mu\nu}$ and a leptonic tensor $L^{\mu\nu}$, as

$$\overline{|\mathcal{M}|^2} = \frac{e^2}{Q^4} L^{\mu\nu} H_{\mu\nu}, \tag{6}$$

where e is the positron charge. We have

$$H_{\mu\nu} = \frac{1}{2} \sum_{\text{spins}} H_\mu^\dagger H_\nu, \tag{7}$$

where

$$\begin{aligned} H_\mu = \overline{u}(p') \big(& F_1 \gamma_\mu P_L + F_2 \gamma_\mu P_R + F_3 p_\mu P_L \\ & + F_4 p_\mu P_R + F_5 p'_\mu P_L + F_6 p'_\mu P_R \big) u(p), \end{aligned} \tag{8}$$

with helicity projectors $P_{L,R} = (1 \mp \gamma^5)/2$ and form factors $F_1, \ldots, F_6$, which follow from the explicit evaluation of the Feynman diagrams shown in Fig. 2 and their counterparts for an incoming charm quark. The leptonic tensor may be decomposed into transverse and longitudinal components, as

$$L^{\mu\nu} = \frac{Q^2}{y^2} \left\{ [1 + (1-y)^2] \epsilon_T^{\mu\nu} - 4(1-y) \epsilon_L^{\mu\nu} \right\}, \tag{9}$$

where

$$\begin{aligned} \epsilon_T^{\mu\nu} &= -g^{\mu\nu} + \frac{4Q^2}{(Q^2 + m_t^2)^2} p^\mu p^\nu + \frac{2}{Q^2 + m_t^2} (p^\mu q^\nu + p^\nu q^\mu), \\ \epsilon_L^{\mu\nu} &= -\frac{1}{Q^2} \left(\frac{2Q^2}{Q^2 + m_t^2} p^\mu + q^\mu \right) \left(\frac{2Q^2}{Q^2 + m_t^2} p^\nu + q^\nu \right). \end{aligned} \tag{10}$$

To obtain the transversal and longitudinal parts of the cross section, the hadron tensor is contracted with the transversal and longitudinal parts of the lepton tensor, respectively.

We generate and evaluate the Feynman diagrams in Fig. 2, with the virtual-photon leg amputated, with the help of the program packages *FeynArts* [8,9] and *FormCalc* [9,10]. We work in 't Hooft-Feynman gauge and use dimensional regularisation to extract the ultraviolet (UV) divergences. We perform the Passarino-Veltman reduction and calculate the squared amplitude (6) using the program package *FeynCalc* [11]. For the numerical evaluation of the standard scalar one-loop integrals, we employ the program package *LoopTools* [10,12]. We perform the numerical integration with the aid of the program package *Cuba* [13]. As a check, we also calculate the amplitude of process (2) with the help of the program package *FeynCalc* and by hand. All three independent calculations are found to lead to the same result. Furthermore, we verify the cancellation of the UV divergences, current conservation, and the reality of the squared amplitude.

2.2 Photoproduction

In the photoproduction limit, the virtual photon is considered as real, with $Q^2 = 0$, so that the longitudinal part of the cross section vanishes. In turn, its energy distribution is described in the Weizsäcker-Williams approximation by the electron-to-photon splitting function

$$f_\gamma(y) = \frac{\alpha}{2\pi}\left[\frac{1+(1-y)^2}{y}\ln\frac{Q^2_{\mathrm{cut}}}{Q^2_{\mathrm{min}}} + 2ym_e^2\left(\frac{1}{Q^2_{\mathrm{cut}}} - \frac{1}{Q^2_{\mathrm{min}}}\right)\right], \tag{11}$$

where $\alpha = e^2/(4\pi)$ is Sommerfeld's fine-structure constant, m_e is the electron mass, and $Q^2_{\mathrm{min}} = y^2 m_e^2/(1-y)$ corresponds to the kinematic lower bound. Thus, the cross section of process (2) in photoproduction is given by

$$\left(\frac{d\sigma}{dy}\right)_{\mathrm{part}} = f_\gamma(y)\sigma_\gamma(y), \tag{12}$$

with

$$\sigma_\gamma = \frac{\pi}{\xi y S}\overline{|\mathcal{M}_\gamma|^2}\delta(\xi y S - m_t^2), \tag{13}$$

where $\mathcal{M}_\gamma$ is the amplitude of $\gamma q \to t$. The kinematically allowed range of y is

$$\frac{m_t^2}{S} < y < y_{\mathrm{max}}. \tag{14}$$

The hadronic cross section is again obtained by convoluting the partonic cross section for a given incoming quark with the corresponding PDF and summing over the incoming-quark flavours. Here, the only candidate mass scale for μ_F is of order m_t, and it is plausible to choose $\mu_F = m_t/2$ so that there is a smooth transition between photoproduction and electroproduction. Again, we have $\mu_F \gg m_c$, so that the use of a charm PDF is justified.

3 Minimal and non-minimal flavour violation in the MSSM

In the MSSM, there are two sources of FC phenomena [14]. The first one is due to flavour mixing in the quark sector, just as in the SM. It is produced by the different flavour rotations in the up- and down-quark sectors, and its strength is driven by the off-diagonal CKM matrix elements. This mixing produces FC electroweak (EW) interaction terms involving CCs, now also involving charged Higgs bosons, and SUSY EW interaction terms of the chargino-quark-squark type. Thus, the SM Feynman diagrams of Fig. 2 are supplemented by those shown in Fig. 3, in which either charged Higgs bosons and down-type quarks or charginos and down-type squarks circulate in the loops. In the MFV MSSM, this is the only source of FC phenomena beyond the SM.

The second source of FC phenomena, which is present in the NMFV MSSM, is due to the possible misalignment between the rotations that diagonalise the quark and squark sectors. When the squark mass matrix is expressed in the basis where the squark fields are parallel to the quark fields (the super CKM basis), it is in general non-diagonal in flavour space. This quark-squark misalignment produces new FC terms in NC as well as in CC interactions. In the SUSY QCD sector, the FC interaction terms involve

NCs of the gluino-quark-squark type. In the case of process (2), this gives rise to the additional Feynman diagrams shown in the first row of Fig. 4. In the SUSY EW sector, the FC interaction terms involve NCs of the neutralino-quark-squark and the chargino-quark-squark type. The first type appears exclusively due to quark-squark misalignment, as in the SUSY-QCD case, whereas the second type receives contributions from both sources, quark-squark misalignment and CKM mixing. The additional Feynman diagrams involving neutralino-quark-squark interactions are displayed in the second row of Fig. 4.

In order to simplify our analysis in the NMFV MSSM, we take the CKM matrix to be diagonal, so that SM contributions (cf. Fig. 2) and the genuine MFV-MSSM contributions, i.e. the charged-Higgs-quark contributions and the part of the chargino-squark contributions due to CKM mixing (cf. Fig. 3), are zero. We are then left with the gluino-squark and neutralino-squark contributions (cf. Fig. 4) and the residual chargino-squark contributions.

Furthermore, we assume that the non-CKM squark mixing is significant only for transitions between the second- and third-generation squarks, and that there is only left-left (LL) mixing, given by an ansatz similar as in Ref. [15], where it is proportional to the product of the SUSY masses involved. This assumption is theoretically well motivated by the flavour-off-diagonal squark squared-mass entries that are radiatively induced via the evolution from high energies down to the EW scale according to the renormalisation group equations (RGEs) [16]. These RGEs predict that the FC LL entries scale with the square of the soft-SUSY-breaking masses, in contrast with the left-right (LR) or right-left (RL) and the right-right (RR) entries, which scale with one or zero powers, respectively. Thus, the hierarchy LL ≫ LR, RL ≫ RR is usually assumed. The same estimates also indicate that the LL entry for the mixing between the second- and third-generation squarks is the dominant one due to the larger quark-mass factors involved. On the other hand, the LR and RL entries are experimentally more constrained, mainly by $b \to s\gamma$ data [17]. With the previous assumption, the squark squared-mass matrices in the $(\tilde{u}_L, \tilde{c}_L, \tilde{t}_L, \tilde{u}_R, \tilde{c}_R, \tilde{t}_R)$ and $(\tilde{d}_L, \tilde{s}_L, \tilde{b}_L, \tilde{d}_R, \tilde{s}_R, \tilde{b}_R)$ bases can be written as follows:

$$M^2_{\tilde{u}} = \begin{pmatrix} M^2_{L,u} & 0 & 0 & m_u X_u & 0 & 0 \\ 0 & M^2_{L,c} & \lambda^t_{LL} M_{L,c} M_{L,t} & 0 & m_c X_c & 0 \\ 0 & \lambda^t_{LL} M_{L,c} M_{L,t} & M^2_{L,t} & 0 & 0 & m_t X_t \\ m_u X_u & 0 & 0 & M^2_{R,u} & 0 & 0 \\ 0 & m_c X_c & 0 & 0 & M^2_{R,c} & 0 \\ 0 & 0 & m_t X_t & 0 & 0 & M^2_{R,t} \end{pmatrix}, \tag{15}$$

$$M^2_{\tilde{d}} = \begin{pmatrix} M^2_{L,d} & 0 & 0 & m_d X_d & 0 & 0 \\ 0 & M^2_{L,s} & \lambda^b_{LL} M_{L,s} M_{L,b} & 0 & m_s X_s & 0 \\ 0 & \lambda^b_{LL} M_{L,s} M_{L,b} & M^2_{L,b} & 0 & 0 & m_b X_b \\ m_d X_d & 0 & 0 & M^2_{R,d} & 0 & 0 \\ 0 & m_s X_s & 0 & 0 & M^2_{R,s} & 0 \\ 0 & 0 & m_b X_b & 0 & 0 & M^2_{R,b} \end{pmatrix}, \tag{16}$$

where

$$\begin{aligned} M^2_{L,q} &= M^2_{\tilde{Q},q} + m_q^2 + \cos(2\beta) M_Z^2 \left(T_3^q - Q_q s_w^2 \right), \\ M^2_{R,q} &= M^2_{\tilde{U},q} + m_q^2 + \cos(2\beta) Q_q s_w^2 M_Z^2 \qquad (q = u, c, t), \\ M^2_{R,q} &= M^2_{\tilde{D},q} + m_q^2 + \cos(2\beta) Q_q s_w^2 M_Z^2 \qquad (q = d, s, b), \end{aligned}$$

$$X_q = A_q - \mu(\tan\beta)^{-2T_3^q}, \tag{17}$$

and λ_{LL}^t and λ_{LL}^b measure the squark flavour mixing strengths in the $\tilde{t}$–$\tilde{c}$ and $\tilde{b}$–$\tilde{s}$ sectors, respectively. As for the SM parameters, m_q, T_3^q, and Q_q are the mass, weak isospin, and electric charge of quark q; M_Z is the Z-boson mass; and $s_w = \sin\theta_w$ is the sine of the weak mixing angle θ_w. As for the MSSM parameters, $\tan\beta = v_2/v_1$ is the ratio of the vacuum expectation values of the two Higgs doublets; μ is the Higgs-higgsino mass parameter; A_q are the trilinear Higgs-sfermion couplings; and $M_{\tilde{Q},q}$, $M_{\tilde{U},q}$, and $M_{\tilde{D},q}$ are the scalar masses. Owing to SU(2)$_L$ invariance, we have $M_{\tilde{Q},u} = M_{\tilde{Q},d}$, $M_{\tilde{Q},c} = M_{\tilde{Q},s}$, and $M_{\tilde{Q},t} = M_{\tilde{Q},b}$. Further MSSM input parameters include the EW gaugino masses M_1 and M_2, the gluino mass M_3, and the mass M_{A^0} of the CP-odd neutral Higgs boson A^0.

In order to reduce the NMFV-MSSM parameter space, we make the following simplifying assumptions. We assume that the flavour mixing strengths in the $\tilde{t}$–$\tilde{c}$ and $\tilde{b}$–$\tilde{s}$ sectors coincide and put $\lambda = \lambda_{LL}^t = \lambda_{LL}^b$ for a simpler notation. Obviously, the choice $\lambda = 0$ represents the case of zero squark flavour mixing. We assume that the various trilinear Higgs-sfermion couplings coincide and write $A_0 = A_u = A_c = A_t = A_d = A_s = A_b$. We assume that the scalar masses coincide thus defining the common SUSY mass scale $M_0 = M_{\tilde{Q},q} = M_{\tilde{U},\{u,c,t\}} = M_{\tilde{D},\{d,s,b\}}$. As for the gaugino masses, we impose the GUT relation $M_1 = (5/3)(s_w^2/c_w^2)M_2$, where $c_w^2 = 1 - s_w^2$, while we treat the gluino mass parameter M_3 as independent. We are thus left with eight independent MSSM parameters, namely, $\tan\beta$, M_{A^0}, M_0, M_2, M_3, A_0, μ, and λ.

4 Numerical analysis

In this section, we present our numerical results. We adopt the SM parameters from Ref. [18] and the effective masses of the down-type quarks from Ref. [19]:

$$\begin{aligned}
&\alpha = 1/137.035\,999\,11, \qquad \alpha_s = 0.117\,6, \\
&(\hbar c)^2 = 0.389\,379\,323\ \mathrm{GeV}^2\mathrm{mb}, \qquad m_e = 0.510\,998\,918\ \mathrm{MeV}, \\
&M_W = 80.403\ \mathrm{GeV}, \qquad M_Z = 91.187\,6\ \mathrm{GeV}, \qquad m_t = 172.7\ \mathrm{GeV}, \\
&m_d = 0.041\ \mathrm{GeV}, \qquad m_s = 0.15\ \mathrm{GeV}, \qquad m_b = 4.5\ \mathrm{GeV}.
\end{aligned} \tag{18}$$

Here, m_t and m_b correspond to pole masses, while m_d and m_s were determined so that their insertion in the perturbative formula for the vacuum polarisation function of the photon reproduces the result extracted from the total cross section of hadron production in e^+e^- annihilation, measured as a function of the CM energy, using a subtracted dispersion relation. This set of quark masses is especially appropriate for quantitative studies in electroweak physics and is frequently employed in the literature. It is used here for definiteness and convenience. As a matter of principle, the precise definition of quark mass is not yet fixed in an analysis of leading order (LO) in QCD like ours. In fact, the freedom of choice of quark-mass definition contributes to the theoretical uncertainty. We employ the standard complex parametrisation of the CKM matrix in terms of three angles θ_{12}, θ_{23}, θ_{13} and a phase δ_{13},

$$V = \begin{pmatrix} c_{12}c_{13} & s_{12}c_{13} & s_{13}e^{-i\delta_{13}} \\ -s_{12}c_{23} - c_{12}s_{23}s_{13}e^{i\delta_{13}} & c_{12}c_{23} - s_{12}s_{23}s_{13}e^{i\delta_{13}} & s_{23}c_{13} \\ s_{12}s_{23} - c_{12}c_{23}s_{13}e^{i\delta_{13}} & -c_{12}s_{23} - s_{12}c_{23}s_{13}e^{i\delta_{13}} & c_{23}c_{13} \end{pmatrix}, \tag{19}$$

where $c_{ij} = \cos\theta_{ij}$ and $s_{ij} = \sin\theta_{ij}$, and adopt from Ref. [18] the values

$$s_{12} = 0.227\,2, \qquad s_{23} = 0.042\,2, \qquad s_{13} = 0.004\,0, \qquad \delta_{13} = 1.00. \tag{20}$$

As for the proton PDFs, we employ the LO set CTEQ6L1 [20] by the Coordinated Theoretical-Experimental Project on QCD (CTEQ) Collaboration. We choose the factorisation scale to be $\mu_F = \left(\sqrt{Q^2} + m_t\right)/2$, with the understanding that $Q^2 = 0$ in the case of photoproduction. At HERA II, electrons or positrons of energy $E_e = 27.6$ GeV collide with protons of energy $E_p = 920$ GeV in the laboratory frame, yielding a CM energy of $\sqrt{S} = 319$ GeV.

4.1 Standard Model

Figures 5 and 6 refer to the SM. Figure 5 shows the total cross section of process (1) as well as its photoproduction and electroproduction components as functions of $\sqrt{S}$. We observe that, for our choice of Q^2_{cut}, the contribution due to photoproduction is approximately twice as large as the one due to electroproduction. At the CM energy of HERA, the cross section is of order 10^{-10} fb and thus many orders of magnitude too small to be measurable. A possible future electron-proton supercollider that uses the HERA proton beam with energy $E_p = 920$ GeV and the electron beam of the international linear e^+e^- collider (ILC) with energy $E_e = 500$ GeV would have a CM energy of 1357 GeV. At this energy, the cross section is of order 10^{-8} fb and likewise not measurable.

Figure 6 shows the Q^2 distribution of the electroproduction cross section as well as its transversal and longitudinal parts. We observe that the transversal part makes the major contribution.

4.2 MSSM with minimal flavour violation

For definiteness, we assume that SUSY is broken according to the mSUGRA scenario of a Grand Unified Theory (GUT). We assign the following default values to the mSUGRA input parameters at the GUT scale:

$$\begin{aligned} &\tan\beta = 56, \qquad m_0 = 1.25\ \text{TeV}, \qquad m_{1/2} = 140\ \text{GeV}, \\ &A_0 = -260\ \text{GeV}, \qquad \text{sign}(\mu) = +1, \end{aligned} \tag{21}$$

where m_0 is the universal scalar mass, $m_{1/2}$ is the universal gaugino mass, and A_0 is the universal trilinear Higgs-sfermion coupling. These values approximately maximise the cross section of process (1) and are in accordance with the experimental bounds from $b \to s\gamma$ decay and on the masses of the various SUSY particles [18]. We calculate the MSSM mass spectrum with the help of the program package *SuSpect* [21].

Figures 7–10 all show the total cross section of process (1) in the MFV MSSM. Specifically, Fig. 7 displays the $\sqrt{S}$ dependence, also separately for the photoproduction and electroproduction contributions, while Figs. 8–10 exhibit, for HERA experimental conditions, the dependencies on $\tan\beta$, $m_{1/2}$, and A_0, respectively, also separately for the charged-Higgs-boson and chargino contributions.

From Fig. 7 we observe that the cross section is of order 10^{-5} fb at HERA energy and of order 10^{-3} fb for the future electron-proton supercollider mentioned above. Both values are too small to yield measurable results.

From Fig. 8 we learn that, as $\tan\beta$ approaches its upper limit, the cross section strongly increases and is mainly generated by the loop diagrams involving charged Higgs bosons. For small values of $\tan\beta$, the SM contribution ($\approx 10^{-10}$ fb) is dominant. Negative interference effects between the charged-Higgs, chargino, and SM contributions can be seen at large values of $\tan\beta$.

From Fig. 9 we see that, as $m_{1/2}$ approaches its lower limit, the cross section strongly increases and is essentially made up by the charged-Higgs-boson contribution alone. The latter is dominant throughout the whole $m_{1/2}$ range, but there are negative interference effects for all values of $m_{1/2}$. The significant suppression of the chargino contribution for $\tan\beta = 56$ familiar from Fig. 8 is actually present for all values of $m_{1/2}$.

As is evident from Fig. 10, the cross section is largest for $A_0 = -260$ GeV and falls off by one (two) orders of magnitude as A_0 reaches -1 TeV (1 TeV). However, the variation with A_0 is less significant than those with $\tan\beta$ and $m_{1/2}$. For $\tan\beta = 56$, the chargino contribution is several orders of magnitude smaller than the charged-Higgs one and almost independent of A_0.

We conclude that, in the MFV MSSM, the mSUGRA scenario characterised by the input parameter values specified in Eq. (21) approximately maximises the cross section of process (1), which still comes out much below the threshold of observability at HERA and a future electron-proton supercollider.

4.3 MSSM with non-minimal flavour violation

Prior to presenting our NMFV-MSSM results, we explain our choice of input parameters. Scanning the eight-dimensional parameter space defined at the end of Section 3, we find that the following assignments, which we henceforth take as default, approximately maximise the cross section of process (1):

$$\begin{aligned} &\tan\beta = 8, \qquad M_{A^0} = 170\text{ GeV}, \qquad M_0 = 475\text{ GeV}, \qquad M_2 = 655\text{ GeV},\\ &M_3 = 195\text{ GeV}, \qquad A_0 = 950\text{ GeV}, \qquad \mu = 345\text{ GeV}, \qquad \lambda = 0.73. \end{aligned} \tag{22}$$

These parameters are in accordance with the lower bounds on the squark masses of 100 GeV and with the experimental lower bounds for the masses of the other SUSY particles [18]. They are also in accordance with the experimental bounds from $b \to s\gamma$ decay [18]. We calculate the MSSM spectrum using the program package *FeynHiggs* [22].

Figures 11–14 all show the total cross section of process (1) in the NMFV MSSM. Specifically, Fig. 11 displays the $\sqrt{S}$ dependence, also separately for the photoproduction and electroproduction contributions, while Figs. 12–14 exhibit, for HERA experimental conditions, the dependencies on λ, M_0, and M_3, respectively. In Figs. 12 and 13, also the contributions from loops involving gluinos, charginos, and neutralinos are shown separately.

From Fig. 11 we read off values of order 10^{-4} fb and 10^{-1} fb for the cross sections at HERA and the future electron-proton supercollider mentioned above, respectively, which is discouraging in the case of HERA and challenging for the electron-proton supercollider, depending on its luminosity.

From Fig. 12 we observe that the cross section strongly increases with λ, by five orders of magnitude as λ runs from 0 to 0.73. For $\lambda > 0.73$, the mass of the lightest squark is less than the lower limit of 100 GeV. The cross section is almost exhausted by the gluino contribution. This may be understood by observing that the corresponding Feynman diagrams are enhanced by a factor of α_s/α relative to those of the chargino and neutralino contributions. The neutralino contribution exhibits a λ dependence similar to the full cross section, but is more than four orders of magnitude smaller. The chargino contribution oscillates about a mean value of 10^{-10} fb in the λ range considered. For $\lambda \lesssim 0.3$ ($\lambda \gtrsim 0.3$), it overshoots (undershoots) the neutralino contribution.

From Fig. 13 we observe that the cross section strongly decreases with increasing value of M_0, by more than three orders of magnitude as M_0 runs from 475 GeV to 2 TeV. The dominant role of the gluino contribution observed in Fig. 12 attenuates in the large-M_0 regime, where the chargino contribution gains influence. Nevertheless, there is a clear hierarchy among the gluino, chargino, and neutralino contributions for $M_0 \gtrsim 700$ GeV, the latter one being least important. For $M_0 \lesssim 700$ GeV, the neutralino contribution exceeds the chargino one. The chargino and neutralino contributions exhibit minima at 650 GeV and 850 GeV, respectively.

From Fig. 14 we learn that the cross section decreases by about two orders of magnitude as M_3 runs from 195 GeV, the Tevatron search limit [18], to 2 TeV.

5 Conclusion

In this paper, the photoproduction and photonic electroproduction of single top quarks in electron-proton scattering was analysed for the first time. The analysis was performed at one loop in the SM as well as the MSSM with minimal and non-minimal flavour mixing. In all three models, the cross section turned out to be too small to be measurable at HERA. The physics at HERA remains interesting because, in the light of our results, the single-top-quark-like events seen by the H1 Collaboration might be a sign of physics not only beyond the SM, but also beyond the MSSM with conserved R parity.

Acknowledgements

We are grateful to John Collins for useful communications regarding Ref. [6]. The work of B.A.K. was supported in part by the German Research Foundation DFG through the Collaborative Research Center No. 676 *Particles, Strings and the Early Universe—the Structure of Matter and Space-Time* and by the German Federal Ministry for Education and Research BMBF through Grant No. 05 HT6GUA.

References

[1] H1 Collaboration, A. Aktas et al., Eur. Phys. J. C 33 (2004) 9;
D.M. South, on behalf of the H1 Collaboration, in: Proceedings of the 14th International Workshop on Deep Inelastic Scattering (DIS 2006), Tsukuba, Japan, 20–24 April 2006 (World Scientific, Singapore, 2007) p. 325.

[2] ZEUS Collaboration, S. Chekanov et al., Phys. Lett. B 559 (2003) 153;
M. Corradi, on behalf of the ZEUS Collaboration, in: Proceedings of the 14th International Workshop on Deep Inelastic Scattering (DIS 2006), Tsukuba, Japan, 20–24 April 2006 (World Scientific, Singapore, 2007) p. 321.

[3] T. Stelzer, Z. Sullivan, S. Willenbrock, Phys. Rev. D 56 (1997) 5919;
S. Moretti, K. Odagiri, Phys. Rev. D 57 (1998) 3040.

[4] F. Gabbiani, E. Gabrielli, A. Masiero, L.Silvestrini, Nucl. Phys. B 477 (1996) 321;
M. Misiak, S. Pokorski, J.Rosiek, Adv. Ser. Direct. High Energy Phys. 15 (1998) 795.

[5] N.G. Deshpande, G. Eilam, Phys. Rev. D 26 (1982) 2463;
S.-P. Chia, G. Rajagopal, Phys. Lett. B 156 (1985) 405;
J.M. Soares, A. Barroso, Phys. Rev. D 39 (1989) 1973;
A. Barroso, Phys. Rev. D 42 (1990) 901;
C.-H. Chang, X.-Q. Li, J.-X. Wang, M.-Z. Yang, Phys. Lett. B 313 (1993) 389.

[6] J.C. Collins, Phys. Rev. D 58 (1998) 094002.

[7] B.A. Kniehl, L. Zwirner, Nucl. Phys. B 621 (2002) 337.

[8] J. Küblbeck, M. Böhm, A. Denner, Comput. Phys. Commun. 60 (1990) 165;
T. Hahn, Comput. Phys. Commun. 140 (2001) 418.

[9] T. Hahn, C. Schappacher, Comput. Phys. Commun. 143 (2002) 54.

[10] T. Hahn, M. Pẽrez-Victoria, Comput. Phys. Commun. 118 (1999) 153.

[11] R. Mertig, M. Böhm, A. Denner, Comput. Phys. Commun. 64 (1991) 345.

[12] T. Hahn, Acta Phys. Polon. B 30 (1999) 3469;
T. Hahn, Nucl. Phys. B (Proc. Suppl.) 89 (2000) 231;
T. Hahn, Nucl. Phys. B (Proc. Suppl.) 157 (2006) 236.

[13] T. Hahn, Comput. Phys. Commun. 168 (2005) 78.

[14] A.M. Curiel, M.J. Herrero, W. Hollik, F. Merz, S. Peñaranda, Phys. Rev. D 69 (2004) 075009;
S. Heinemeyer, W. Hollik, F. Merz, S. Peñaranda, Eur. Phys. J. C 37 (2004) 481.

[15] T.P. Cheng, M. Sher, Phys. Rev. D 35 (1987) 3484.

[16] K. Hikasa, M. Kobayashi, Phys. Rev. D 36 (1987) 724;
P. Brax, C.A. Savoy, Nucl. Phys. B 447 (1995) 227.

[17] M. Ciuchini, E. Franco, A. Masiero, L. Silvestrini, Phys. Rev. D 67 (2003) 075016;
M. Ciuchini, E. Franco, A. Masiero, L. Silvestrini, Phys. Rev. D 68 (2003) 079901 (Erratum).

[18] Particle Data Group, W.-M. Yao et al., J. Phys. G 33 (2006) 1.

[19] A. Denner, Fortschr. Phys. 41 (1993) 307.

[20] J. Pumplin, D.R. Stump, J. Huston, H.L. Lai, P. Nadolsky, W.-K. Tung, JHEP 07 (2002) 012.

[21] A. Djouadi, J.-L. Kneur, G. Moultaka, Comput. Phys. Commun. 176 (2007) 426.

[22] S. Heinemeyer, W. Hollik, G. Weiglein, Comput. Phys. Commun. 124 (2000) 76.

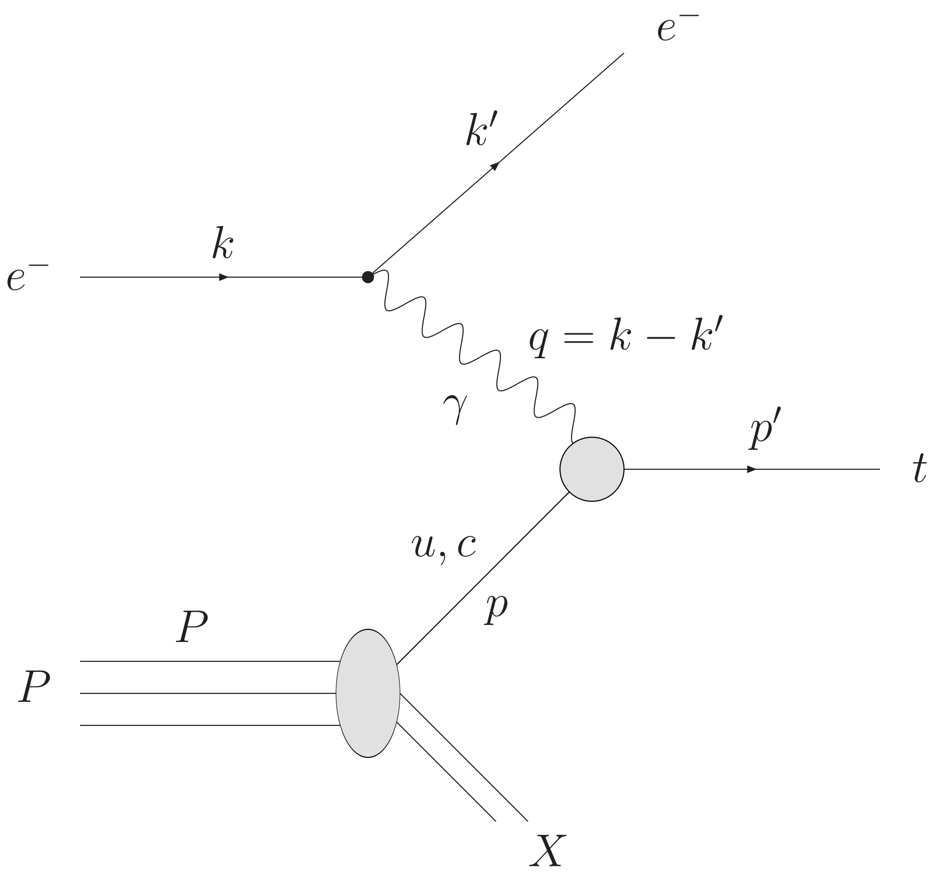

Figure 1: Schematic representation of the hadronic process (1) explaining the four-momentum assignments.

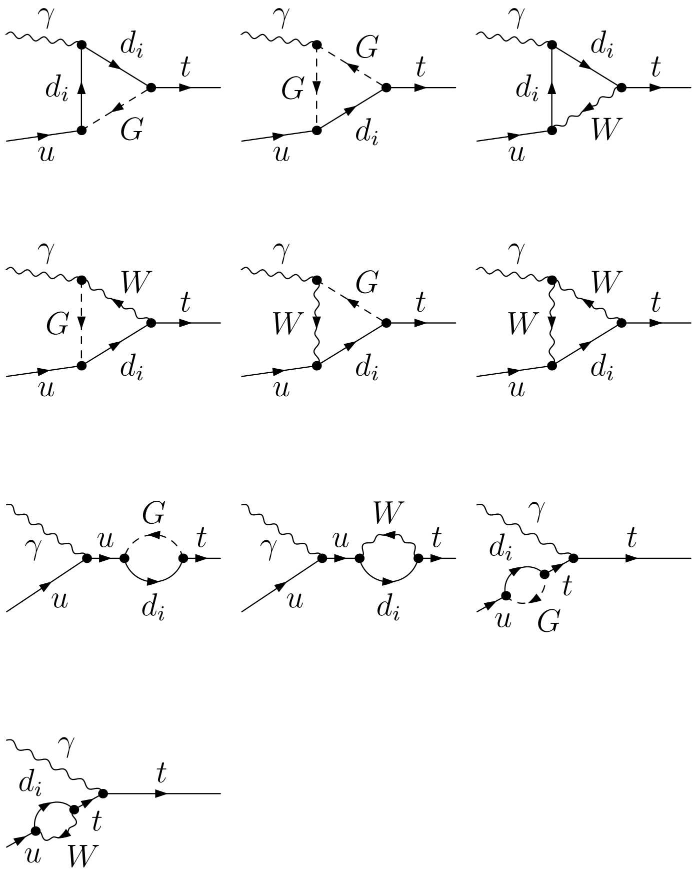

Figure 2: Feynman diagrams of partonic subprocess (2) in the SM. Here, G is the charged Goldstone boson and d_i with $i = 1, 2, 3$ are the down-type quarks.

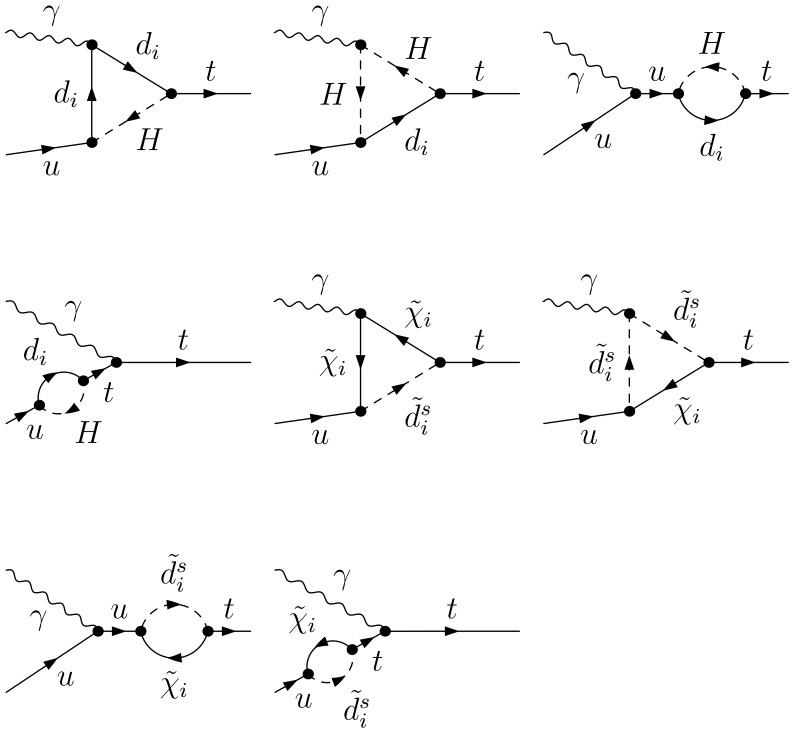

Figure 3: Additional Feynman diagrams of partonic subprocess (2) arising in the MFV MSSM. Here, $\tilde{d}_i^s$ with $i = 1, 2, 3$ and $s = 1, 2$ are the down-type squarks, and $\tilde{\chi}_i$ with $i = 1, 2$ are the charginos.

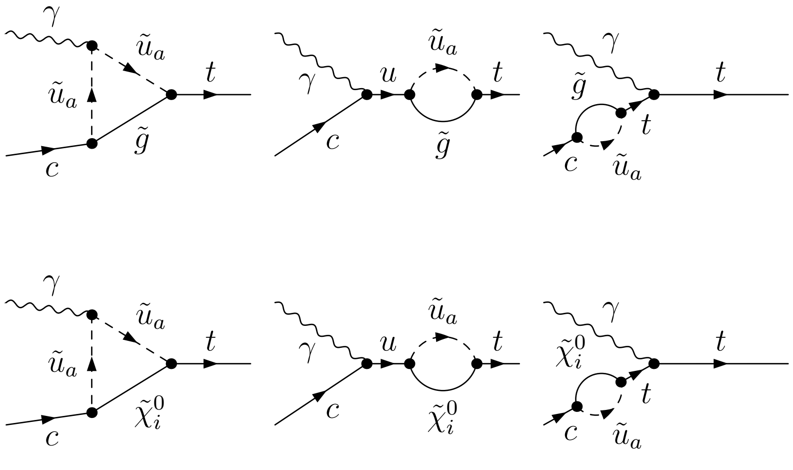

Figure 4: Additional Feynman diagrams of partonic subprocess (2) arising in the NMFV MSSM. Here, $\tilde{g}$ is the gluino, $\tilde{u}_a$ with $a = 1, \ldots, 6$ are the up-type squarks, and $\tilde{\chi}_i^0$ with $i = 1, \ldots, 4$ are the neutralinos.

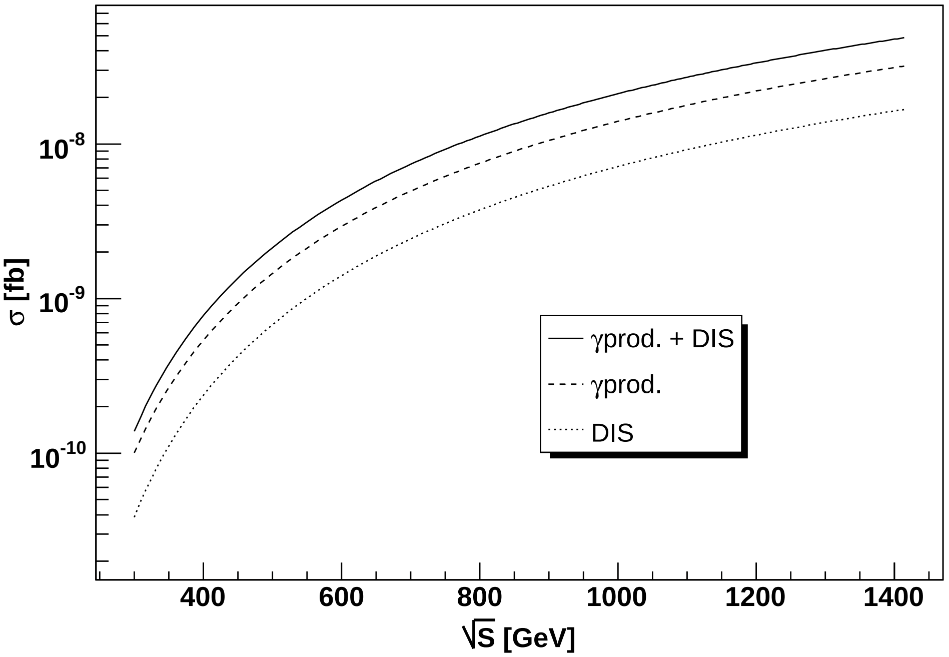

Figure 5: Total cross section and its photoproduction and electroproduction parts in the SM as functions of $\sqrt{S}$.

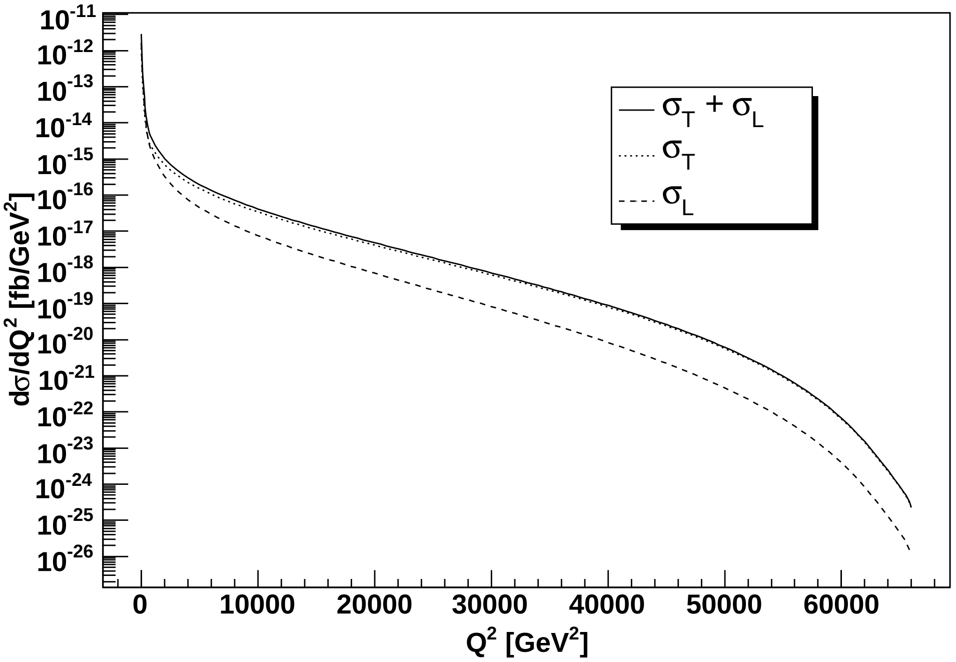

Figure 6: Q^2 distribution of the cross section and its transversal and longitudinal parts in the SM under HERA experimental conditions.

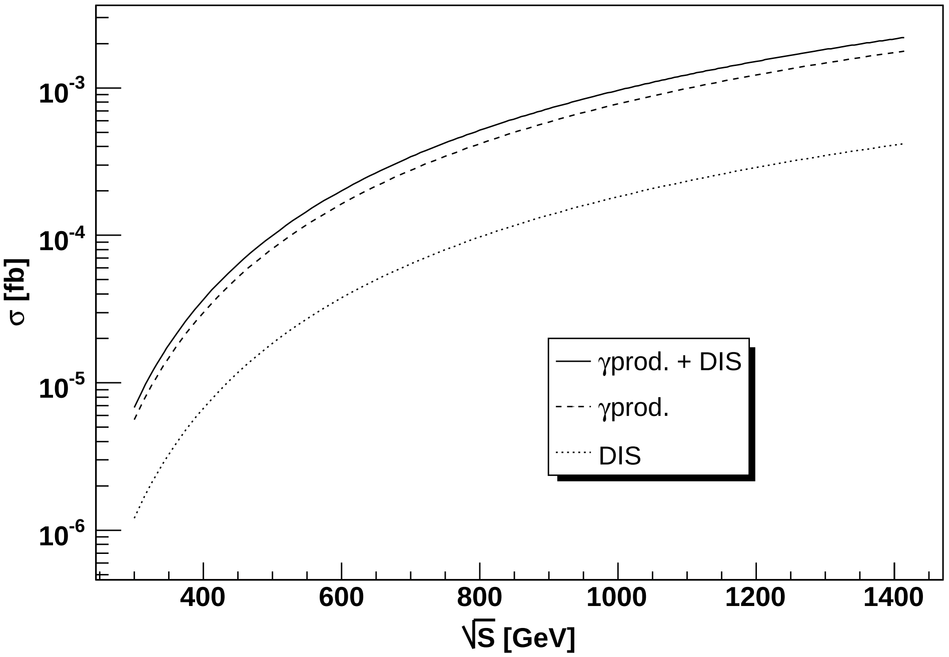

Figure 7: Total cross section and its photoproduction and electroproduction parts in the MFV MSSM as functions of $\sqrt{S}$.

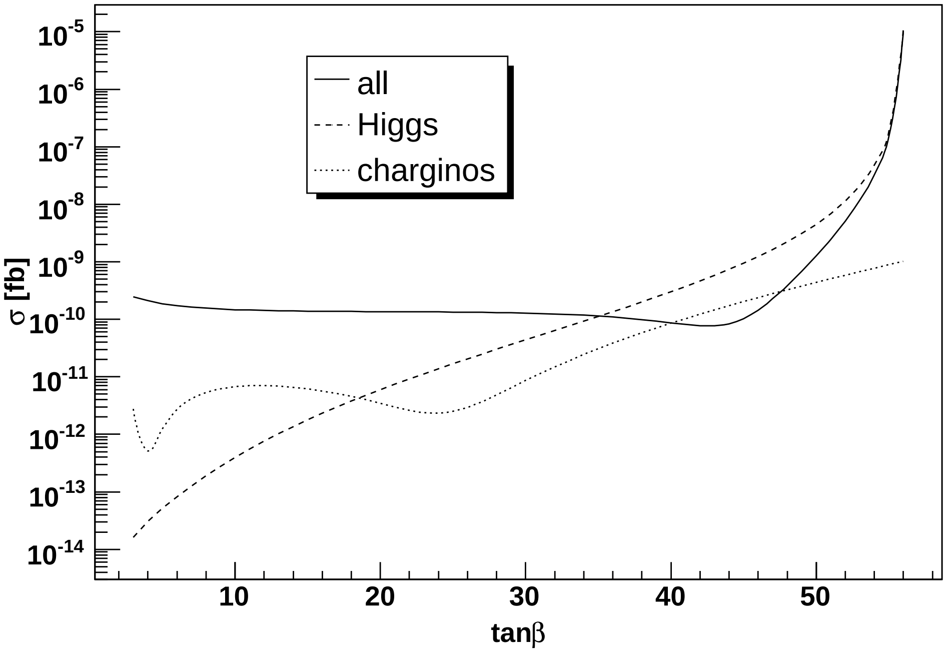

Figure 8: Total cross section and its Higgs and chargino parts in the MFV MSSM as functions of $\tan\beta$ under HERA experimental conditions.

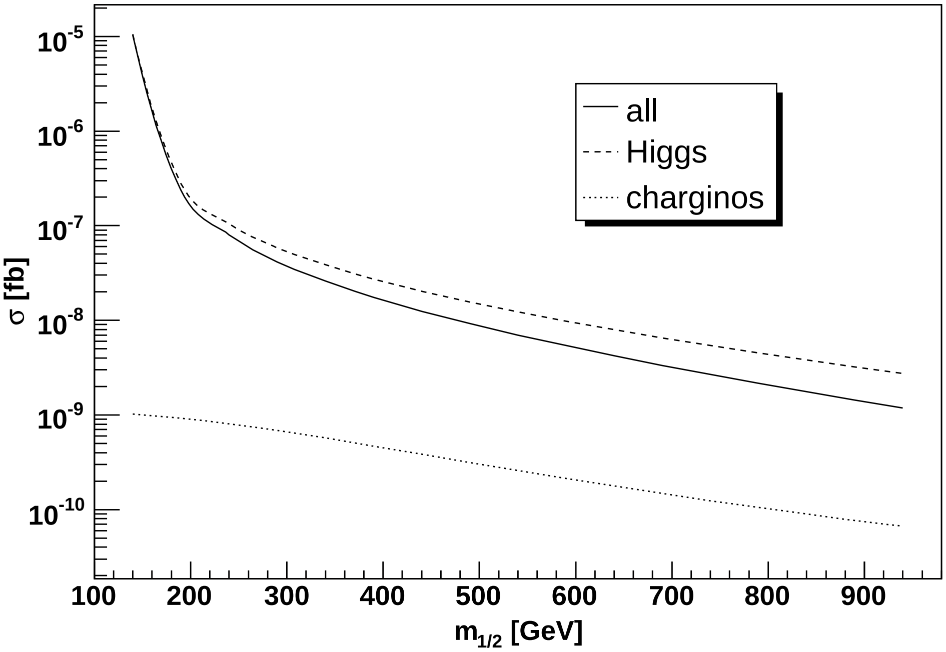

Figure 9: Total cross section and its Higgs and chargino parts in the MFV MSSM as functions of $m_{1/2}$ under HERA experimental conditions.

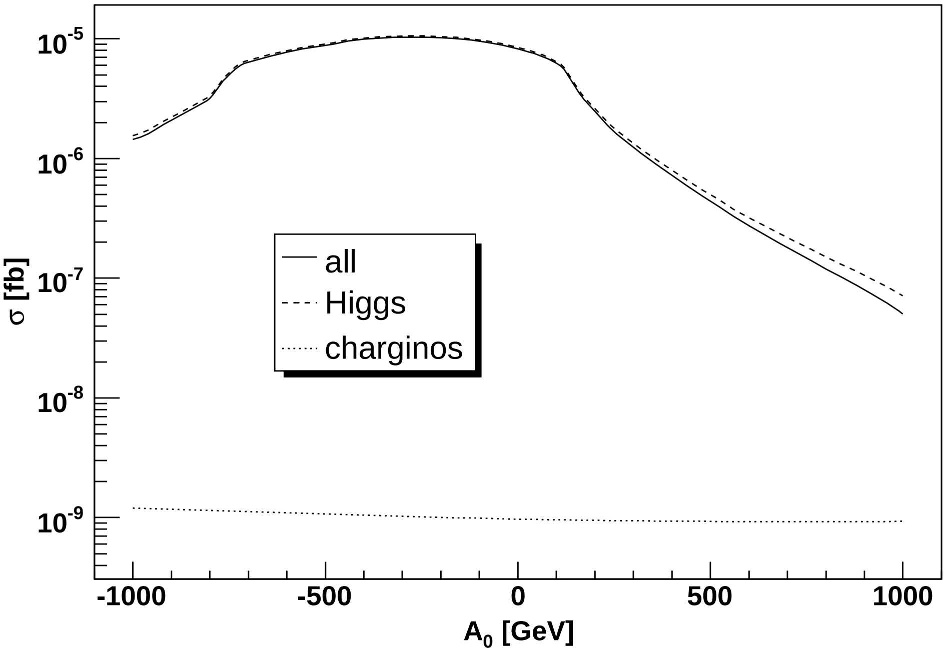

Figure 10: Total cross section and its Higgs and chargino parts in the MFV MSSM as functions of A_0 under HERA experimental conditions.

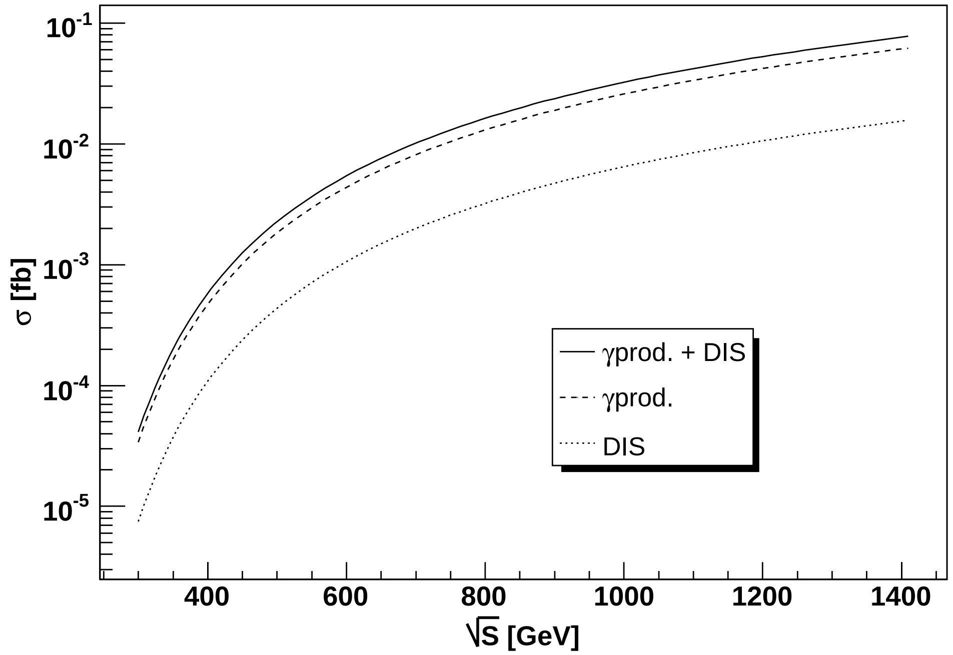

Figure 11: Total cross section and its photoproduction and electroproduction parts in the NMFV MSSM as functions of $\sqrt{S}$.

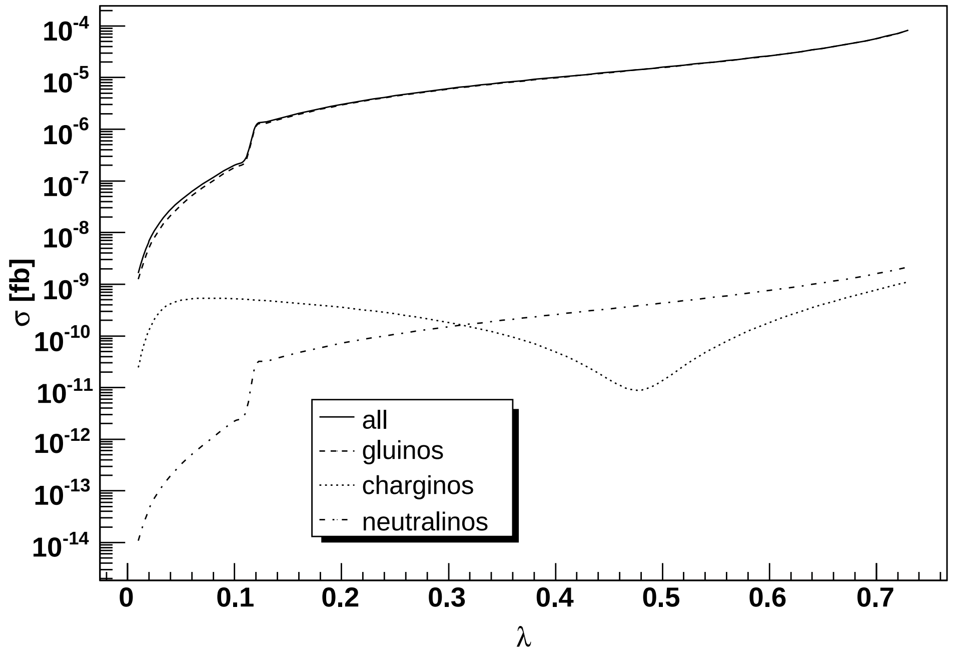

Figure 12: Total cross section and its gluino, chargino, and neutralino parts in the NMFV MSSM as functions of λ under HERA experimental conditions.

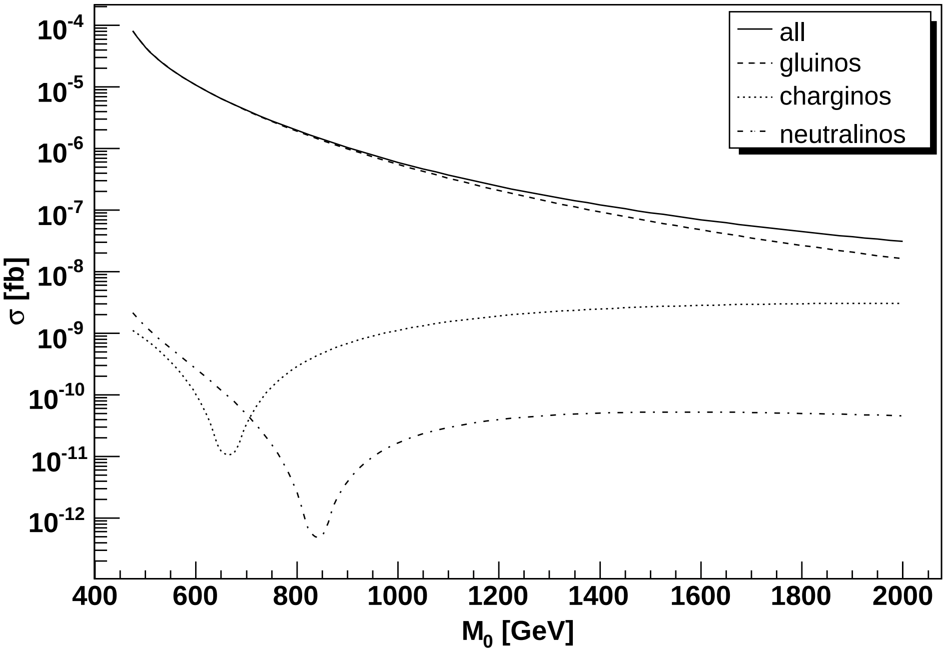

Figure 13: Total cross section and its gluino, chargino, and neutralino parts in the NMFV MSSM as functions of M_0 under HERA experimental conditions.

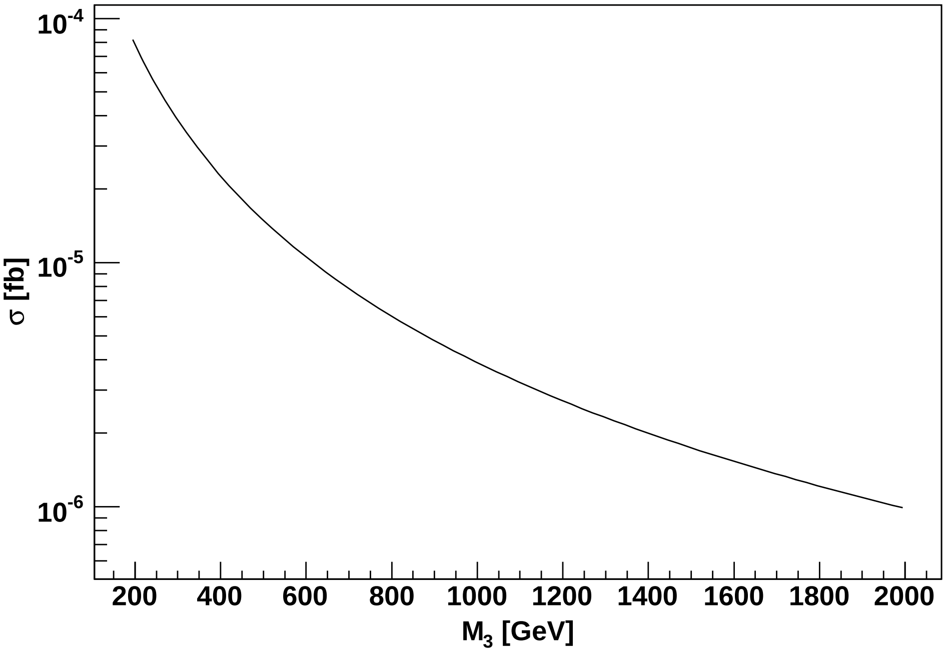

Figure 14: Total cross section in the NMFV MSSM as function of M_3 under HERA experimental conditions.